Journal of Electroanalytical Chemistry 886 (2021) 115122

Contents lists available at ScienceDirect

Journal of Electroanalytical Chemistry

journal homepage: www.elsevier.com/locate/jelechem

A novel visible light photoelectrochemical aptasensor for determination of bisphenol A based on surface plasmon resonance of gold nanoparticles activated g-C_3N_4 nanosheets

Behjat Deiminiat, Gholam Hossein Rounaghi *

Department of Chemistry, Faculty of Sciences, Ferdowsi University of Mashhad, Mashhad, Iran

ARTICLE INFO

Keywords:
Photoelectrochemical aptasensor
Label-free
Bisphenol A
Graphitic carbon nitride
Gold nanoparticles

ABSTRACT

A novel visible light photoelectrochemical (PEC) aptasensor was fabricated for label-free determination of bisphenol A (BPA) using graphitic carbon nitride (g-C_3N_4) nanosheets and gold nanoparticles (AuNPs). The flourin tin-oxide (FTO) glass plates were prepared by spray pyrolysis method and they were modified with g-C_3N_4 and AuNPs. The SH-terminal aptamer was then adsorbed on the surface of AuNPs /g-C_3N_4/FTO electrode through formation of thiol–gold (S–Au) bonds. In the presence of bisphenol A molecules, the structure of the aptamer molecules changes to G-quadruplex which limits the electron transfer on the electrode surface. Cyclic voltammetry (CV), electrochemical impedance spectroscopy (EIS) and time-based photocurrent measurements were carried out to investigate the changes of the surface of the FTO electrode in each step. Under the optimal experimental conditions, the constructed PEC aptasensor displayed a linear response to bisphenol A within the concentration range of 0.1–1000 nM with a detection limit of 0.03 nM. The PEC aptasensor did not show any cross-reactivity towards the analogues which are similar to BPA molecules. In addition, the proposed aptasensor was employed for determination the low concentration of BPA in real samples such as mineral water, milk, baby bottle, food storage container and urine with satisfactory results.

1. Introduction

Bisphenol A (BPA) is an endocrine-disruptor chemical which is mainly used in the production of polycarbonate and epoxy resins [1]. The wide usage of the BPA-based materials, has been resulted in the release of a large quantities of this compound into the environment [2,3]. BPA can also migrate into the beverages and foods from the plastic packaging of the products under the heat, pressure and acidic or basic conditions [4,5]. In body, BPA mimics the physiological function of the estrogen hormone, occupies the hormonal receptors and disrupts the synthesis and metabolism of the estrogen [6,7]. It has been proven that BPA has the adverse effects on the human health and it can cause the sexual dysfunction, birth defect, impaired immune function and also enhanced cancer risk [8,9]. Thus, the detection and quantification of BPA is very important for human health and safety. Different analytical methods such as gas chromatography-mass spectrometry, gas chromatography- tandem mass spectrometry, liquid chromatography-mass spectrometry, high performance liquid chromatography-tandem mass spectrometry, enzyme-linked immune sorbent assay (ELISA) and electrochemical methods have been used for determination of BPA in various types of samples [10–15]. Among the above-mentioned techniques, the electrochemical methods have demonstrated to be sensitive and reliable for measurement the concentration of BPA in solutions. However, the strongly adsorption of intermediates at the surface of the electrodes during the oxidation of BPA, decreases the sensitivity of this electrochemical sensors [16].

Recently, photoelectrochemical (PEC) technique has gained much attention as a new analytical method due to its high sensitivity and low background signals [17–19]. In the PEC method, a light source is used to excite a photoactive modified electrode, and the produced photocurrent is used as a detection signal. The PEC detection technique, possesses the benefits of both optical and electrochemical methods owing to the complete separation of the light source and detection signal [20]. Several semiconductors such as TiO_2, CeO_2, ZnO and CdS have been used as the photoactive nanomaterials for the fabrication of PEC sensors [21–24]. Among them, TiO_2 has been widely employed in the PEC sensing due to its high physical and chemical stability,

* Corresponding author.
E-mail address: ronaghi@um.ac.ir (G.H. Rounaghi).

https://doi.org/10.1016/j.jelechem.2021.115122
Received 2 December 2020; Received in revised form 26 February 2021; Accepted 27 February 2021
Available online 9 March 2021

excellent photochemical property, biocompatibility and low cost. However, TiO_2 has a large energy band gap (3.2 eV) and only shows photocatalytic activity under the UV illumination which limits its application [25–27].

Graphitic carbon nitride (g-C_3N_4) is a polymeric semiconductor that has been used as a novel photoactive nanomaterial in different fields such as water splitting, photodegradation of pollutants, fuel cells, photosynthesis of organic compounds and also construction of biosensors. This is because it has an interesting electronic structure with the visible light band gap of 2.69 eV, nontoxic nature and also high thermal and chemical stability [28–31].

In order to improve further the performance of the PEC sensors, biorecognition elements such as aptamers have been combined with the PEC technique [32]. Aptamers are artificial single-stranded DNA or RNA oligonucleotides which are prepared in vitro using the systematic evolution of ligands by exponential enrichment (SELEX) technique [33]. Aptamers are able to bind to a wide range of targets, from small molecules to proteins and even cells with a high specificity [34,35].

In this research work, a highly sensitive and selective photoelectrochemical aptasensor was developed for measurement the concentration of BPA in solution based on AuNPs/g-C_3N_4 nanocomposite film. The graphitic carbon nitride was prepared as a new photoelectrocatalyst and characterized using scanning electron microscopy (SEM), transmission electron microscopy (TEM), energy dispersive X-ray analysis (EDX) and X-ray diffraction analysis (XRD). The PEC aptasensor was fabricated based on the immobilization of aptamer on the surface of AuNPs/g-C_3N_4/FTO electrode via the formation of S–Au bonds between the–SH group of the aptamer and the gold nanoparticles. The developed aptasensor was used for sensitive and selective determination of BPA based on a PEC signal “switch off–on” strategy.

2. Experimental

2.1. Materials

The BPA aptamer with the sequence of 5′-SH-$(CH2)_6$-CCG GTG GGT GGT CAG GTG GGA TAGCGT TCC GCG TAT GGC CCA GCG CAT CAC GGG TTC GCA CCA-3′ was supplied from Sangon Biotechnology company (Shanghai, China). Bisphenol A (BPA) and bisphenol B (BPB) were obtained from Merck chemical company (Darmstadt, Germany). Bisphenol AF (6F-BPA) was purchased from Exir (Germany) and 4,4′-biphenol (BP) was obtained from Alfa Aeser (Germany). Hydrogen tetrachloroaurate trihydrate ($HAuCl_4{\cdot}3H_2O$), tris-(2-carboxyethyl) phosphinehydrochloride (TCEP) and 6-mercapto-1-hexanol (MCH) were purchased from Sigma-Aldrich chemical company (USA). All the other chemicals used in this research work were obtained from Merck (Darmstadt, Germany).

2.2. Apparatus

Electrochemical measurements were performed using a μAutolab electrochemical system model PGSTAT 101 (Metrohm) equipped with a NOVA software. The electrochemical cell was assembled with a platinum wire counter electrode, a saturated Ag/AgCl reference electrode (both electrodes was purchased from Azar electrode, Urmia, Iran) and FTO working electrode. The FTO electrode was prepared by spray coating system (S.C.S. 92, Iran). A 150 W Xe lamp (Osram, Germany) equipped with a UV filter was used as an irradiation source. A Metrohm pH meter (Model 827) was employed for adjustment of pH. The surface morphologies of the prepared FTO electrode and the synthesized g-C_3N_4, were investigated using scanning electron microscope (LEO1450VP). The TEM images of g-C_3N_4 were taken with a LEO 912 AB transmission electron microscope. The XRD patterns of the FTO film and g-C_3N_4 were obtained with an X-ray diffractometer (Explorer GNR-Italy). The elemental analysis was performed by an energy dispersive X-ray microanalyzer (Oxford-7353).

2.3. Preparation of FTO electrode

The spray pyrolysis method was used for the preparation of the FTO electrode [36]. In this method, the glass plates were employed as the electrode substrate. A solution containing 33 g of stannic chloride, 3 g of ammonium fluoride, 40 mL of ethanol and 32 mL of deionized water was prepared with stirring for 1 h. Then, the resulting solution was used for covering the surface of the glass plates with a flourin tin-oxide (FTO) layer by using the spray coating system. The distance between the substrate and nozzle was 35 cm and the rate of spray was 5 mL min^{-1}. The temperature of the substrate was kept at 450 °C and the pressure of the carrier gas was 3 atm.

2.4. Synthesis of graphitic carbon nitride (g-C_3N_4)

The graphitic carbon nitride nanosheets were synthesized by heating of melamine and urea [37]. To this end, 2.5 g of urea and 2.5 g of melamine were mixed thoroughly and the resulting mixture was heated under the following temperature program: from room temperature to 300 °C with the heating rate of 8 °C min^{-1}, from 300 to 500 °C with the heating rate of 2 °C min^{-1} and from 500 to 550 °C with the heating rate of 1 °C min^{-1}. Finally, it was heated for 2 h at 550 °C. After cooling to room temperature, the g-C_3N_4 product was ground into a powder [38,39].

2.5. Fabrication of PEC aptasensor

At first, the FTO plates were cut into 20 × 5 mm^2 pieces and sonicated sequentially in a deionized water and soap solution for 10 min, isopropanol for 5 min, ethanol for 5 min and acetone for 2 min. For fabrication of PEC aptasensor, 5 mg of the synthesized g-C_3N_4 was dispersed in 5 mL of deionized water for 20 min to form a homogeneous suspension and then, 20 μL volume of the prepared suspension was transferred onto the surface of a FTO slice (with a surface area of 0.25 cm^2) and dried under an infrared lamp. The gold nanoparticles were incorporated into the g-C_3N_4 film through cyclic voltammetry from a 1 mM $HAuCl_4$ solution containing 0.1 M KNO_3 by applying potential in a range of − 0.4 V to + 1.2 V for 20 cycles with a scan rate of 50 mV s^{-1}. The aptamer was covalently attached to the gold nanoparticles by self-assembly method. For this purpose, 20 μL aliquot of Tris-HCl solution (10 mM, pH 7.0) containing 1.0 μM aptamer reduced by TCEP for 1 h, was dropped on the surface of AuNPs /g-C_3N_4 modified FTO electrode and the electrode was stored at 4 °C for 16 h. After the allotted time, the electrode was rinsed thoroughly with Tris-HCl solution to remove the unbounded aptamer. Then, 20 μL of MCH solution (2 μM) was dropped on the electrode surface and the modified electrode was kept at room temperature for 1 h to block the nonspecific sites. Finally, the fabricated aptasensor was washed with deionized water, dried under nitrogen stream and it was used for quantitative measurement of BPA molecules in solutions. Fig. 1, shows the stepwise construction process of the proposed PEC apatasensor and its sensing strategy for BPA molecules in solutions.

2.6. Photoelectrochemical measurements

Before each measurement, the binding of the BPA target molecule to its aptamer was performed. For this purpose, 20 μL of binding buffer solution (25 mM Tris-HCl, pH 7.0 with 25 mM KCl, 100 mM NaCl and 10 mM $MgCl_2$) containing appropriate concentration of BPA was added onto the surface of aptamer/AuNPs/g-C_3N_4/FTO electrode and the electrode was incubated at room temperature for 60 min. Then, the electrode was rinsed with Tris-HCl buffer solution to remove the unbonded BPA molecules. The photoelectrochemical measure-

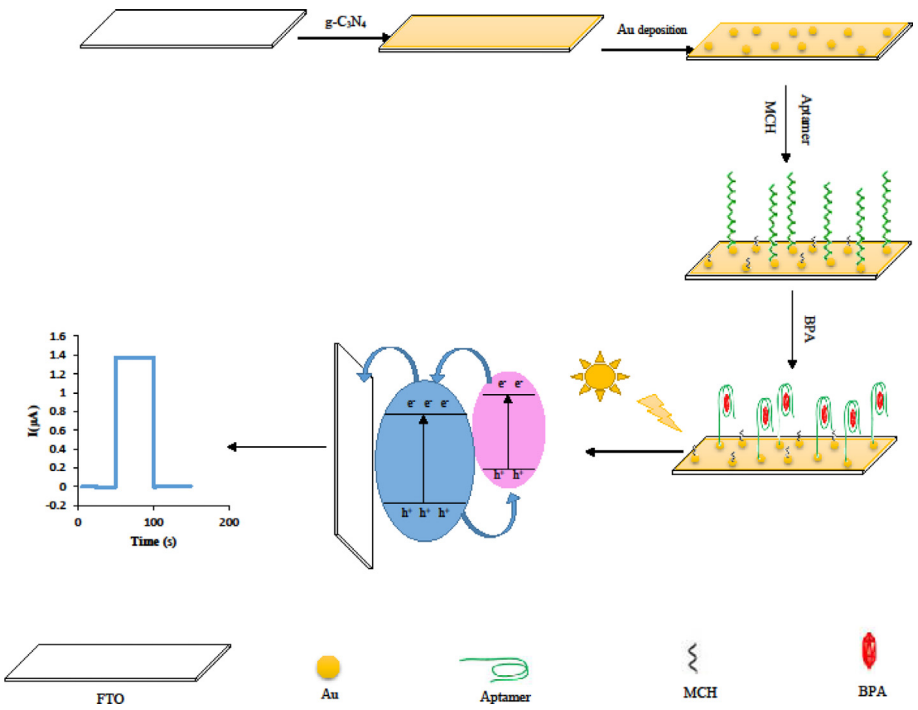

Fig. 1. Schematic illustration of PEC apatasensor construction and the detection mechanism of BPA molecules.

ments were carried out in a phosphate buffer solution (0.1 M, pH 7) at a constant potential of 0.2 V.

2.7. Sample preparation

Commercial food samples with plastic packaging such as mineral water and liquid milk were supplied from a local supermarket in Mashhad, Iran. The mineral water sample was examined without any pretreatment just it was mixed with Tris–HCl buffer solution to increase the ionic strength of the water. Prior to measurement, 5.0 mL of milk sample was mixed with 20 mL of Tris-HCl solution under sonication for 30 min. Then, the prepared mixture was centrifuged for 10 min and the supernatant of the solution was diluted with Tris-HCl solution.

The other samples which include the food storage container and baby bottle were purchased from local markets. The samples were cleaned with water, alcohol and acetone, respectively, and then cut into small pieces. 1.0 g of plastic sample and 30 mL of deionized water were added into a flask. The flask was heated in oil bath at 70 °C for 48 h. Then, the flask was cooled to room temperature and the sample solution was filtered and diluted with Tris-HCl buffer solution.

Urine sample was obtained from a healthy adult and stored at 4 °C before analysis. The sample was centrifuged at 3500 rpm for 10 min and the supernatant was diluted with Tris-HCl buffer solution.

3. Results and discussion

3.1. Characterization of FTO electrode

The surface morphology of the prepared FTO electrode was investigated by scanning electron microscopy (SEM). The SEM image of the FTO electrode shows a spongy and uniform surface (Fig. 2A). For further evaluation, the elemental analysis of the surface of the FTO electrode was performed using energy dispersive X-ray (EDX) technique. The presence of Sn, Si and O elements on the electrode surface was proved by the EDX results (Fig. 2B). The X-ray diffraction (XRD) pattern of the FTO electrode surface was also investigated. The XRD pattern (Fig. 2C), illustrates a tetragonal crystal structure for the prepared FTO film. The higher intensity peak can be attributed to the crystal plane of (200) [36].

3.2. Characterization of the synthesized g-C_3N_4

Scanning electron microscopy (SEM), transmission electron microscopy (TEM), energy dispersive X-ray analysis (EDX) and X-ray diffraction analysis (XRD) were used for characterization of the synthesized g-C_3N_4. Fig. 3A, shows the SEM image of g-C_3N_4. As is evident in this Figure, the g-C_3N_4 seems to have a nanosheet structure. The TEM image of the synthesized g-C_3N_4 is shown in Fig. 3B. Fig. 3C represents the EDX spectrum of the g-C_3N_4 nanosheets. The C and N peaks are clearly seen in this Figure which demonstrates the presence of these two elements at the chemical composition of the synthesized g-C_3N_4. In order to further support the results obtained from SEM, TEM and EDX studies, the XRD pattern of the g-C_3N_4 was also recorded (Fig. 3D). Two diffraction peaks which are appeared at 13.1° and 27.7°, confirm the formation of g-C_3N_4 nanosheets. The sharp peak at 27.7° can be attributed to the (002) diffraction plane of graphitic materials owing to the interlayer stacking of aromatic sections [40]. The peak at 13.1° is indexed as (100) and it can be assigned to the interlayer structural packing motif of tri-s-triazine units [41].

The surface morphology of AuNPs/g-C_3N_4/FTO modified electrode was also investigated by SEM, EDX and XRD techniques. As is evident in Fig. 4A, a homogeneous layer of g-C_3N_4 with well dispersed Au nanoparticles has been coated on the surface of the FTO electrode. The C, N and Au peaks which are obviously seen in the EDX analysis results (Fig. 4B) confirm the chemical composition of the AuNPs/g-C_3N_4/FTO surface. The XRD pattern of the AuNPs/g-C_3N_4/FTO was also recorded (Fig. 4C). FTO shows two diffraction peaks at 37.91° and 51.3°. The peaks which are appeared at 13.1° and 26.5° can be attributed to the diffraction planes of g-C_3N_4 nanosheets. Two diffraction peaks which are seen at 44.1° and 61.6° can be assigned to the Au nanoparticles. Fig. 4D, shows the FT-IR spectrum of the prepared aptamer/AuNPs/g-C_3N_4 film. The formation of Au–S bond between the gold nanoparticles and the thiol group of the aptamer at 5′ end is proven by the stretching vibration peak at 760 cm^{-1} [42].

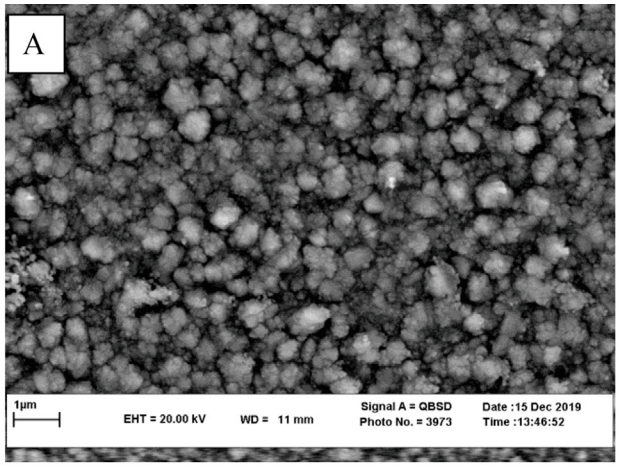

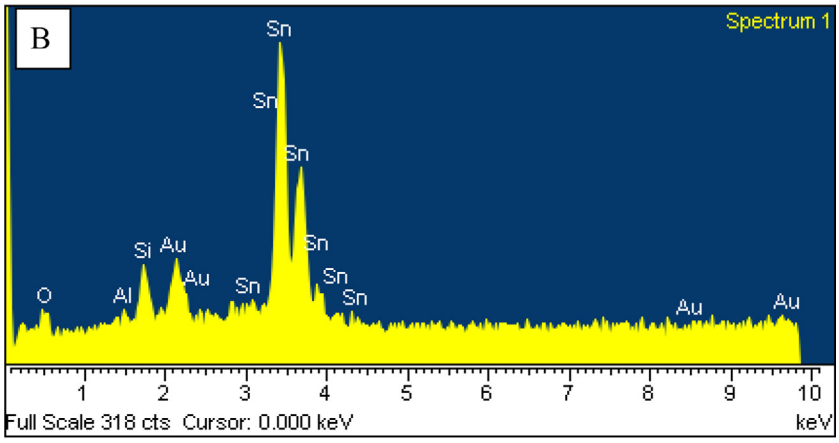

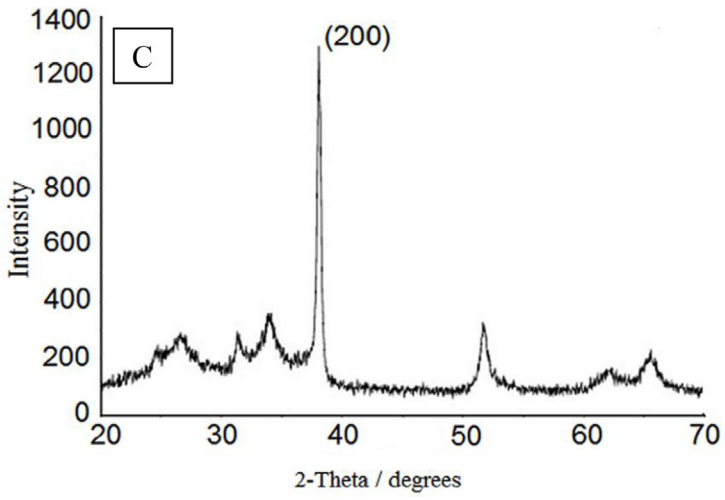

Fig. 2. (A) SEM image, (B) EDX spectrum and (C) XRD pattern of the prepared FTO electrode.

3.3. Electrochemical characterization of PEC aptasensor

Different electrochemical techniques including cyclic voltammetry (CV), electrochemical impedance spectroscopy (EIS) and chronoamperometry were employed to characterize the fabrication process of the proposed PEC aptasensor. Fig. 5A, exhibits the cyclic voltammograms of the FTO electrode at different construction steps in the presence of $[Fe\ (CN)_6]^{3-/4-}$ redox probe. As can be seen in this Figure, the bare FTO electrode shows a pair of peaks for the oxidation and reduction of the probe molecules. When the surface of the FTO electrode is covered with g-C_3N_4 and AuNPs, the intensity of these peaks increases significantly (curves b and c). The reasonable explanation is that the presence of g-C_3N_4 and AuNPs at the electrode surface can increase the specific surface area and also the electrical conductivity of the electrode which enhances the electron transmission of $[Fe(CN)_6]^{3-/4-}$ at the surface of g-C_3N_4/FTO and

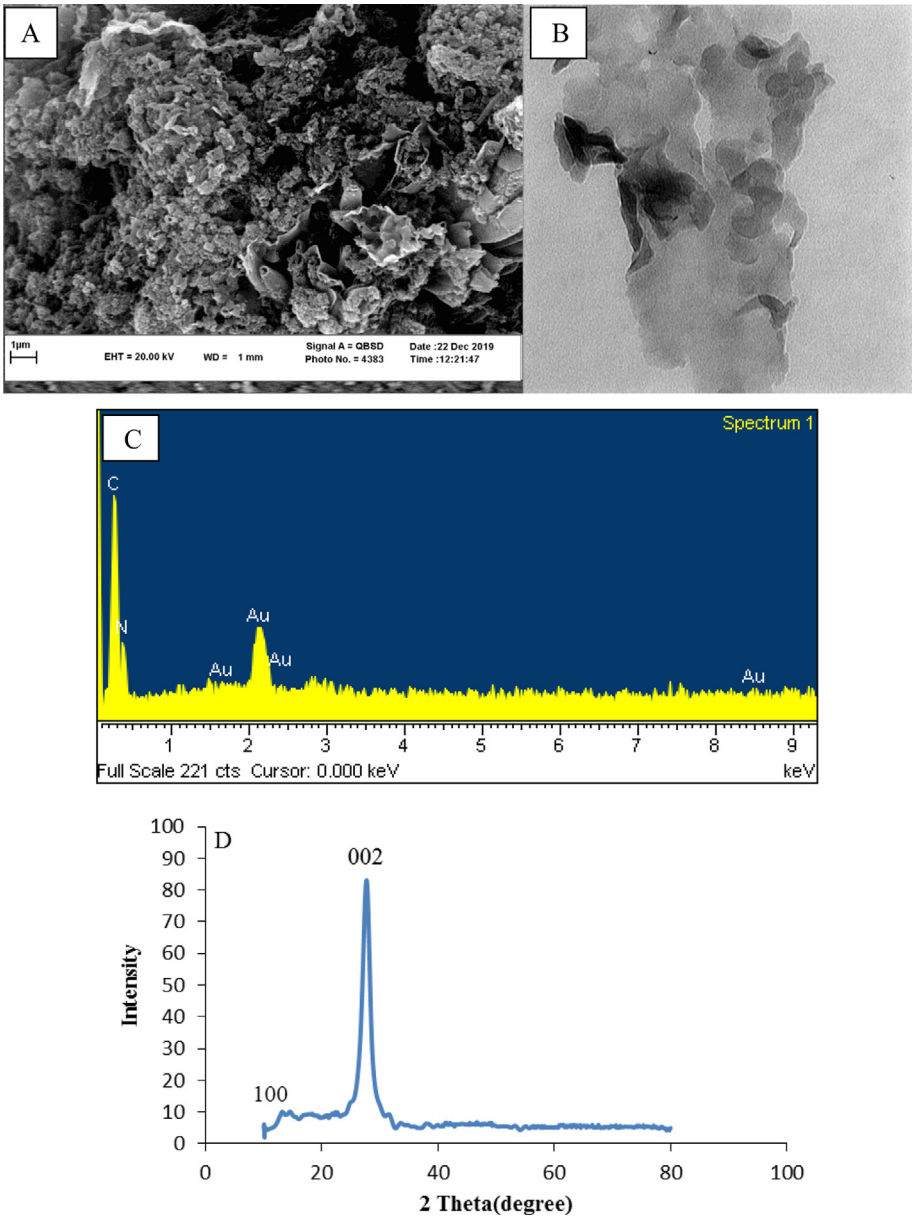

Fig. 3. (A) SEM image, (B) TEM image, (C) EDX spectrum and (D) XRD pattern of the synthesized g-C_3N_4.

AuNPs/g-C_3N_4/FTO modified electrodes. In contrast, after immobilization of the aptamer at the surface of AuNPs/g-C_3N_4/FTO electrode, the peak intensity decreases considerably owing to the electrostatic repulsion force between the negatively charged of the aptamer and $[Fe(CN)_6]^{3-/4-}$ redox probe. With addition of BPA molecules onto the electrode surface, the peak intensity further decreases. This behavior is due to the structural change of the aptamer upon interaction with the BPA molecules which restricts the mass-transfer of the redox probe to the electrode surface which results in a weak electrochemical response.

The Nyquist plots of the bare and modified FTO electrodes recorded in $[Fe(CN)_6]^{3-/4-}$ solution are shown in Fig. 5B. As is seen in Fig. 5B, the charge transfer resistance (R_{et}) value of the bare FTO electrode, is higher than that for g-C_3N_4/FTO modified electrode which indicates a faster electron transfer process at the g-C_3N_4/FTO electrode surface. After electrodeposition of AuNPs on the surface of g-C_3N_4/FTO electrode, the semicircle diameter decreases remarkably and the Nyquist plot shows approximately a straight line. When the BPA aptamer is immobilized onto the surface of modified FTO electrode, the R_{et} value (R_{et} = 370.8) increases compared to AuNPs/g-C_3N_4/FTO electrode (R_{et} = 153), which proves the successful attachment of the aptamer on the surface of AuNPs/g-C_3N_4/FTO electrode. Subsequently, the binding of aptamer to the BPA molecules, results in an obvious increase in R_{et} value. The increase in R_{et} value can be attributed to the change of the aptamer structure after interaction with the target molecules.

Fig. 6, depicts the time-based photocurrent responses of the bare FTO, g-C_3N_4/FTO, AuNPs/g-C_3N_4/FTO, aptamer/AuNPs/g-C_3N4/FTO and BPA/aptamer/AuNPs/g-C_3N_4/FTO electrodes in phosphate buffer solution (0.1 M, pH 7). As is evident in this Figure, no photocurrent response is observed for the bare FTO electrode under radiation of visible light. On the other hand, the g-C_3N_4/FTO and AuNPs/g-C_3N_4/FTO electrodes show the photocurrents of 0.59 and 1.94 µA respectively, upon photo-excitation with the visible light. This increase in the photocurrent response can be explained by this fact that upon irradiation the surface of the electrodes with visible light, the hot electrons are formed in Au nanoparticles due to the surface plasmon resonance (SPR) effect and injected into the conduction band of

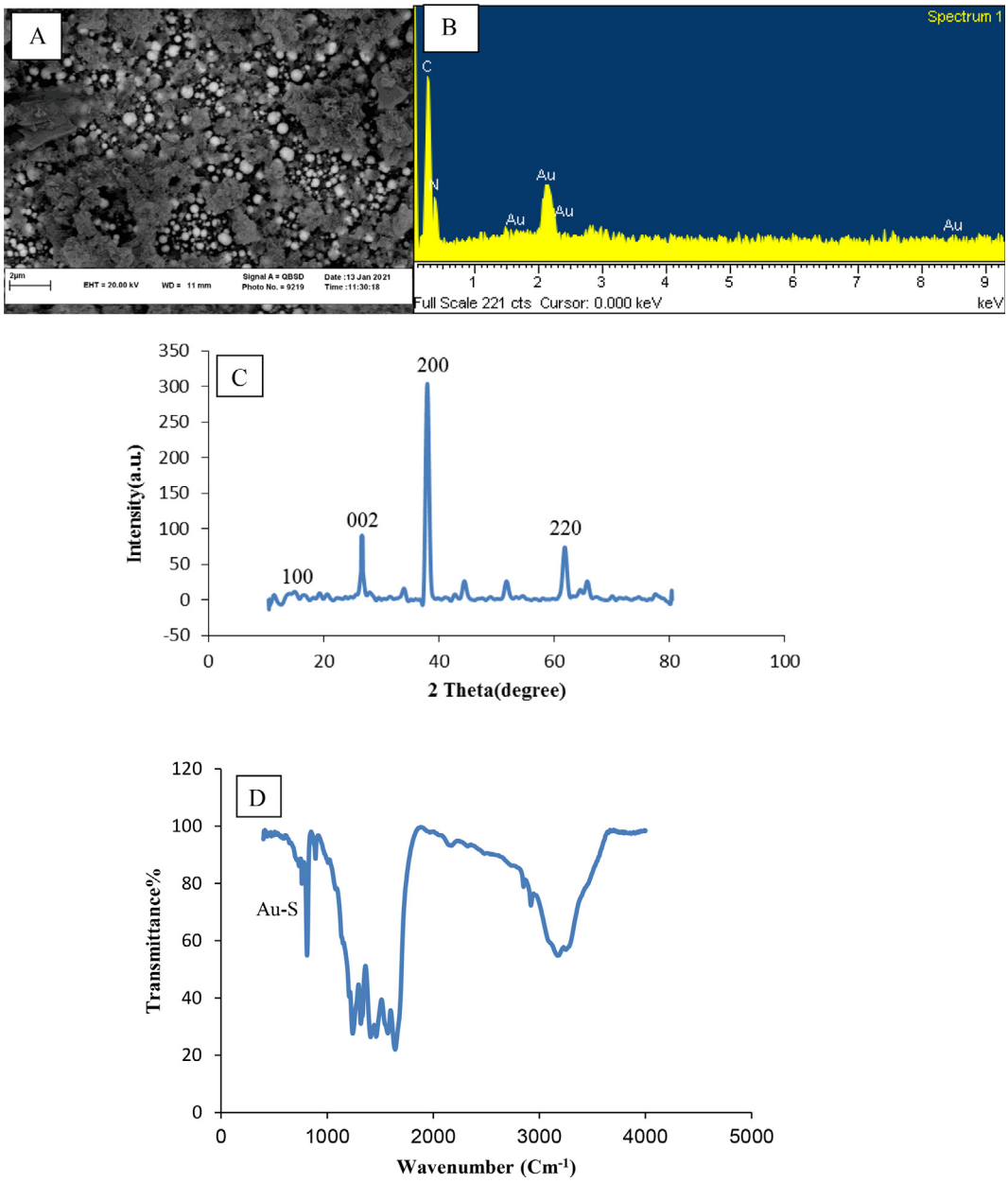

Fig. 4. (A) SEM image, (B) EDX spectrum and (C) XRD pattern of AuNPs/g-C_3N_4/FTO and (D) FT-IR spectrum of aptamer /AuNPs/g-C_3N_4 film.

g-C_3N_4 nanosheets. Moreover, the fast electron transfer from Au nanoparticles to g-C_3N_4 nanosheets, decreases the recombination rate of the photo-generated electron-hole pairs [43,44]. But, when the aptamer is attached onto the surface of AuNPs/g-C_3N_4/FTO electrode, the photocurrent decreases, because the incident light cannot arrive on the electrode surface. Also, the presence of the aptamer at the surface of the electrode, can prevent the electron transfer process [45]. When the prepared PEC apatasensor is exposed to the target molecules, the conformation of the aptamer is changed to G-quadruplex which further decreases the photocurrent response.

3.4. Optimization of the effective parameters on the PEC aptasensor performance

3.4.1. Effect of the aptamer concentration

The aptamer concentration is a key parameter that has an important effect on the photocurrent response of the proposed PEC aptasensor. Fig. 7A, shows that the photocurrent intensity increases with increasing the aptamer concentration loaded on the electrode surface from 0.5 μM to 1.0 μM and then it decreases at higher concentrations which may due to the steric hindrance toward the electron transfer at the electrode surface. Therefore, the aptamer concentration of 1.0 μM was selected as the optimum value for the construction of the proposed PEC aptasensor.

3.4.2. Effect of BPA binding time

The effect of the binding time of BPA molecules to the aptamer on the performance of the fabricated aptasensor was investigated in the time range of 30 to 90 min and the obtained results are depicted in Fig. 7B. As is evident in this Figure, the photocurrent increases with the increment of BPA binding time between 30 and 60 min and then it remains nearly constant with increasing the time which is an evidence for saturation of the aptasensor surface by the BPA molecules. Thus, 60 min was chosen as the optimum time for the binding of BPA molecule to its aptamer.

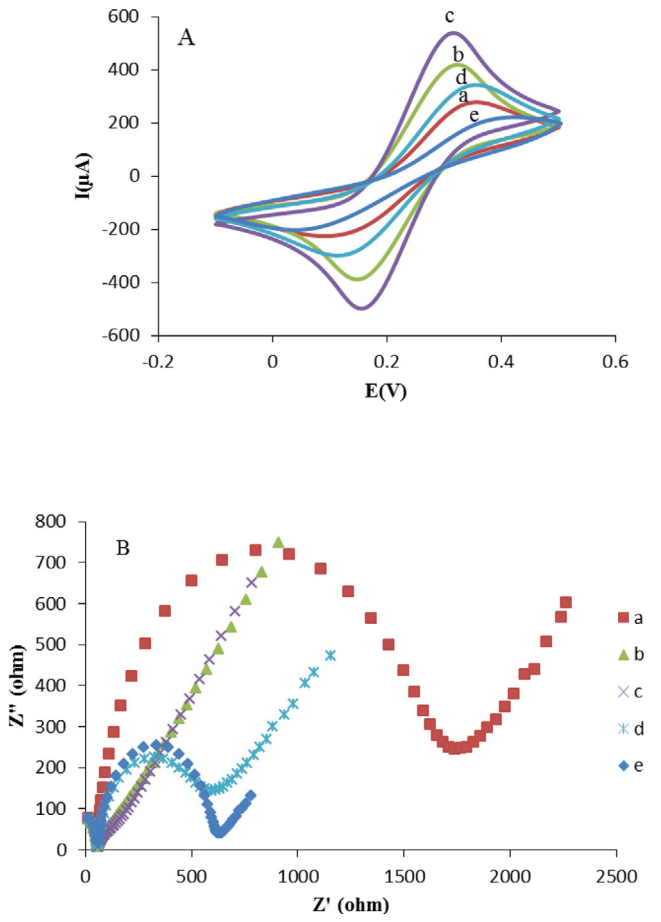

Fig. 5. (A) Cyclic voltammograms and (B) Nyquist plots of (a) bare FTO, (b) g-C_3N_4/FTO, (c) AuNPs/g-C_3N_4/FTO, (d) aptamer/AuNPs/g-C_3N4/FTO and (e) BPA/aptamer/AuNPs/g-C_3N_4/FTO in 0.1 M phosphate buffer solution (pH 7.0) containing 0.1 M KCl and 5.0 mM $K_3[Fe(CN)_6]/K_4$ $[Fe(CN)_6]$. Conditions for CV: Potential scan range −0.1 V to + 0.5 V and scan rate 50 mVs^{-1} and for EIS: potential 0.20 V, frequency range of 0.1–30000 Hz and amplitude of 10 mV.

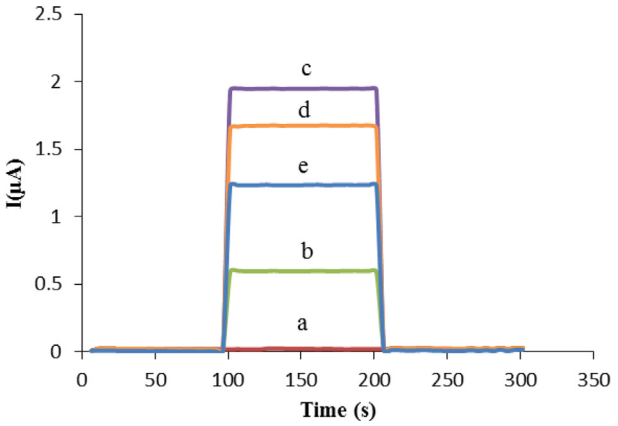

Fig. 6. Time-based photocurrent responses of (a) bare FTO, (b) g-C_3N_4/FTO, (c) AuNPs/g-C_3N_4/FTO, (d) aptamer/AuNPs/g-C_3N4/FTO and (e) BPA/aptamer/AuNPs/g-C_3N_4/FTO under in 0.1 M phosphate buffer solution (pH 7.0) at potential of 0.2 V under radiation of visible light.

3.4.3. Effect of pH

The pH of the binding solution plays an important role in the interaction of BPA molecule with its aptamer and hence the analytical performance of PEC aptasensor. Therefore, the pH of the solution must be optimized. As shown in Fig. 7C, the fabricated aptasensor has a maximum photocurrent intensity at pH 7 because the aptamer is easily inactivated in the high acidic or alkaline media. As a result, pH 7 was selected as a suitable pH for determination the concentration of BPA in solutions.

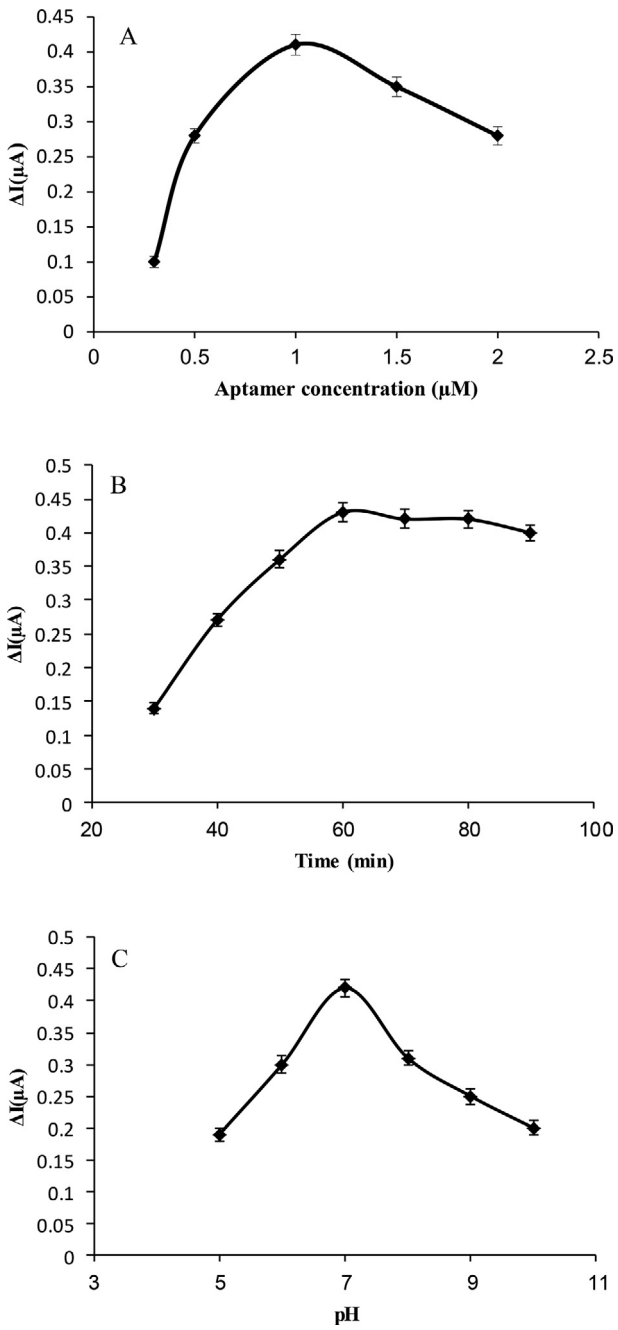

Fig. 7. Effect of (A) aptamer concentration, (B) BPA binding time and (C) pH on the photocurrent response of the PEC aptasensor.

3.5. Analytical performance of the PEC aptasensor

The analytical performance of the proposed PEC aptasensor was investigated by recording the photocurrent responses of the sensor under the visible light illumination. Fig. 8A, shows the photocurrent-time curves of the PEC aptasensor in different concentrations of BPA. As can be seen in this Figure, the photocurrent intensity

decreases with increasing the concentration of BPA in solutions. Fig. 8B, depicts a linear relationship between ΔI and log C in the concentration range from 0.1 to 1000 nM with the regression equation of ΔI (μA) = 0.1713 log C (nM) + 0.4635 and the correlation coefficient of 0.9952. Here, log C is the logarithm of concentration of BPA and ΔI is the photocurrent difference which is calculated by subtracting the photocurrent response recorded in the presence of BPA from the photocurrent response observed in the absence of BPA molecules. The limit of detection (LOD) was found to be 0.03 nM according to $3S_b/S$ relation, in which S_b is the standard deviation of the blank solution for five measurements and S is the slop of calibration plot. The analytical performance of the prepared aptasensor and some of the previously reported BPA electrochemical sensors is compared in Table 1. As is evident in this table, the proposed PEC aptasensor possesses a lower detection limit, as well as, a wider linear range in comparison with the other constructed electrochemical sensors. The good performance of the PEC aptasensor can be attributed to the high binding affinity of the aptamer toward the BPA molecules and also the SPR effect of the gold nanoparticles, which effectively amplifies the photocurrent response of g-C_3N_4 nanosheets under irradiation by the visible light.

3.6. Selectivity, reproducibility and stability of the PEC aptasensor

In order to determine the selectivity of the developed PEC aptasensor, the photocurrent response of the aptasensor was individually measured toward bisphenol A (BPA), bisphenol B (BPB), 4,4′-biphenol (BP) and 6F bisphenol A (6F-BPA) under the same experimental conditions. As can be seen in Fig. 9, the photocurrent response obtained for the BPA molecules, is noticeably higher than that of the interfering species which confirms the excellent selectivity of the fabricated photoelectrochemical aptasensor for determination the concentration of BPA in solutions.

To evaluate the reproducibility of the photoelectrochemical aptasensor, five PEC aptasensors were constructed under the same experimental conditions and they were used for measurement the photocurrent response of BPA in solution. The relative standard deviation (RSD) was found to be 3.3%.

The stability of the prepared PEC aptasensor was also investigated for a two weeks period. For this purpose, the PEC aptasnsor was employed for determination the same concentration of BPA every day. After 14 days, the photocurrent response of the fabricated sensor was retained to 95% of initial value which indicates that the proposed PEC aptasensor possesses a good stability.

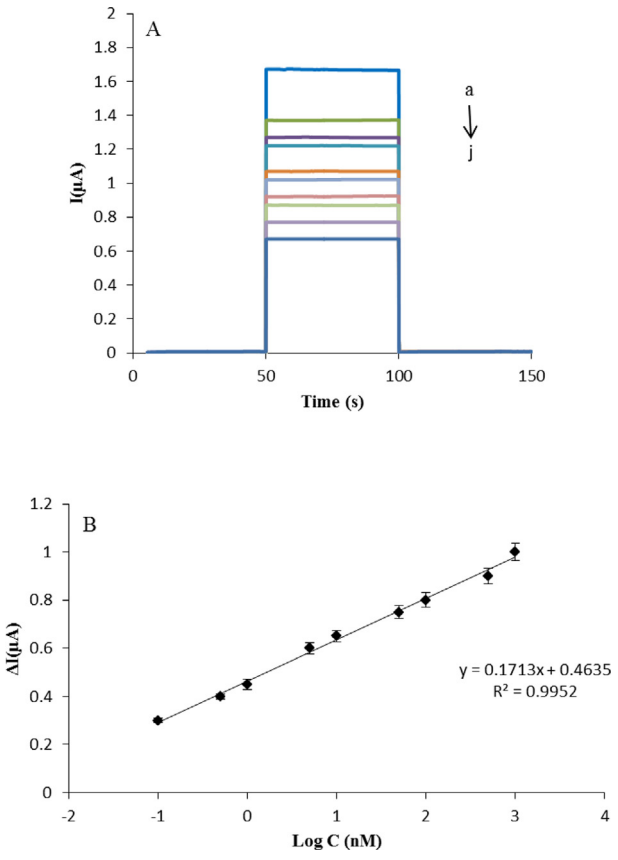

Fig. 8. (A) Time-based photocurrent responses of PEC aptasensor for different concentrations of BPA (from a to j: 0, 0.1, 0.5 1, 5, 10, 50, 100, 500, 1000 nM) and (B) calibration curve of PEC aptasensor. Error bars represent the standard deviations for three replicate measurements.

Table 1
Comparison the analytical performance of different electrochemical sensors for BPA determination in solutions.

Method	Linear range (μmol L^{-1})	Detection limit (μmol L^{-1})	Reference
Cu_2O/rGO/GCE	0.1–80	0.053	[46]
AuNP/MWCNT/GCE	0.01–0.7	0.004	[47]
CS/*N*-GS/GCE	10–1300	0.005	[48]
AuPdNPs/GNs-GCE	0.05–10	0.008	[49]
ELDH/GCE	0.02–1.51	0.0068	[50]
aptamer/AuNPs/g-C_3N_4/FTO	1×10^{-4}–1	3×10^{-5}	This work

3.7. Practical application of the PEC aptasensor

In order to study the applicability of the proposed PEC aptasensor, the photoelectrochemical measurements of BPA were performed in mineral water, milk, baby bottle, food storage container and urine samples. These samples were prepared according to the procedures which are explained in section 2.7, then, they were spiked with appropriate concentrations of BPA standard solution and the photoelectrochemical measurements were carried out using the standard addition method. The values of the recoveries and RSDs obtained from these measurements are listed in Table 2. As is evident in Table 2, these values are in the ranges from 94% to 106% for recovery and from 2.3 to 4.2% for RSD which clearly demonstrates the successful operation of the developed aptasensor for quantitative measurement of BPA in different real sample solutions.

3.8. Conclusion

In this study, a new label free photoelectrochemical aptasensor was constructed for determination the concentration of bisphenol A in solutions. The combination of graphitic carbon nitride as a photoactive nanomaterial, apatamer as a biorecognition element and gold nanoparticles as the photocurrent amplifier, led to increase the sensitivity and selectivity of the fabricated photoelectrochemical sensor. Also, the proposed PEC aptasensor, showed a low detection limit of 0.03 nM, a wide linear range from 0.1 to 1000 nM and a good stability and reproducibility for determination the concentration of BPA in solutions. Moreover, the prepared PEC aptasensor, was successfully used for measurement the trace levels of BPA in mineral water, milk, baby bottle, food storage container and also for an urine sample and the acceptable results were achieved. The acceptable recoveries which were obtained in these measurements, reveal that the matrix of the real samples does not have a considerable effect on the analytical performance of the fabricated sensor and the proposed PEC aptasensor is a promising tool for quantitative determination of BPA in biological, food and plastic samples in the future.

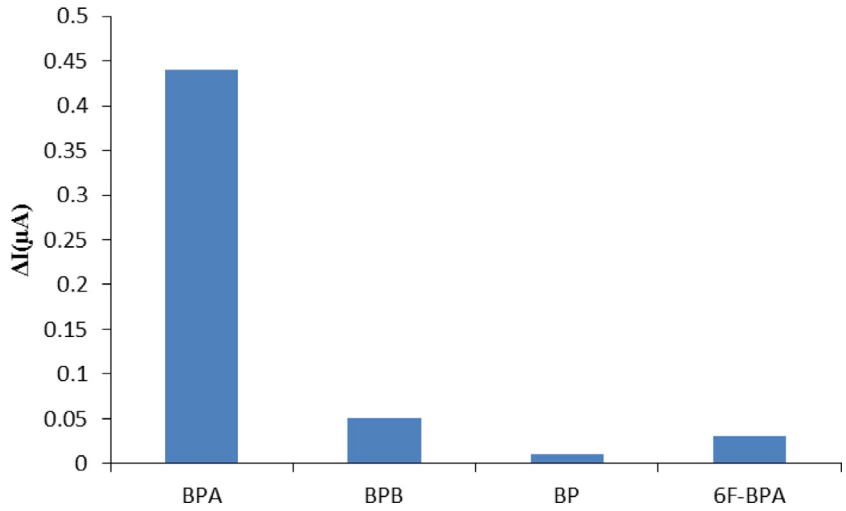

Fig. 9. Selectivity of the proposed PEC aptasensor to BPA molecules and some interferences including BPB, BP and 6F-BPA.

Table 2
Determination of BPA in real samples (n = 3).

Sample	Adedd (nM)	Detected (nM)	Recovery (%)	RSD (%)
	0	Not detected	–	–
Mineral water	0.5	0.51	102	2.7
	1	0.99	99	2.3
	0	Not detected	–	–
Milk	0.5	0.53	106	3.4
	1	0.98	98	3.1
	0	Not detected	–	3.5
Baby bottle	0.5	0.48	96	4.2
	1	1.03	103	3.7
	0	0.45	–	2.8
Food storage	0.5	0.92	94	3.9
container	1	1.46	101	4.1
	0	Not detected	–	–
Urine	0.5	0.49	98	3.0
	1	1.2	102	2.9

CRediT authorship contribution statement

Behjat Deiminiat: Investigation, Writing - original draft, Formal analysis. **Gholam Hossein Rounaghi:** Validation, Writing - review & editing, Supervision, Funding acquisition.

Declaration of Competing Interest

The authors declare that they have no known competing financial interests or personal relationships that could have appeared to influence the work reported in this paper.

Acknowledgments

The authors gratefully acknowledge the support of this research work by Iran National Science Foundation (INSF), Tehran, Iran (97026039) and the gracious help of the Ferdowsi University of Mashhad, Mashhad, Iran.

References

[1] L.N. Vandenberg, M.V. Maffini, C. Sonnenschein, B.S. Rubin, A.M. Soto, Bisphenol-A and the great divide: a review of controversies in the field of endocrine disruption, Endocr. Rev. 30 (2009) 75–95.
[2] J.-H. Kang, F. Kondo, Y. Katayama, Human exposure to bisphenol A, Toxicology 226 (2-3) (2006) 79–89.
[3] H. Fromme, T. Küchler, T. Otto, K. Pilz, J. Müller, A. Wenzel, Occurrence of phthalates and bisphenol A and F in the environment, Water Res. 36 (6) (2002) 1429–1438.
[4] A. Goodson, H. Robin, W. Summerfield, I. Cooper, Migration of bisphenol A from can coatings-effects of damage, storage conditions and heating, Food Addit. Contam. 21 (10) (2004) 1015–1026.
[5] J. López-Cervantes, P. Paseiro-Losada, Determination of bisphenol A in, and its migration from, PVC stretch film used for food packaging, Food Addit. Contam. 20 (6) (2003) 596–606.
[6] J. Xu, L.i. Wang, Y. Zhu, Decontamination of bisphenol A from aqueous solution by graphene adsorption, Langmuir 28 (22) (2012) 8418–8425.
[7] H.S. Chang, K.H. Choo, B. Lee, S.J. Choi, The methods of identification, analysis and removal of endocrine disrupting compounds (EDCs) in water, J. Hazard. Mater. 172 (2009) 1–12.
[8] R. Rezg, S. El-Fazaa, N. Gharbi, B. Mornagui, Bisphenol A and human chronic diseases: current evidences, possible mechanisms, and future perspectives, Environ. Int. 64 (2014) 83–90.
[9] X. Xin, S. Sun, H.e. Li, M. Wang, R. Jia, Electrochemical bisphenol A sensor based on core–shell multiwalled carbon nanotubes/graphene oxide nanoribbons, Sensors Actuat. B Chem. 209 (2015) 275–280.
[10] S.C. Cunha, J.O. Fernandes, Assessment of bisphenol A and bisphenol B in canned vegetables and fruits by gas chromatography-mass spectrometry after QuEChERS and dispersive liquid-liquid microextraction, Food Control 33 (2) (2013) 549–555.
[11] Y. Deceuninck, E. Bichon, S. Durand, N. Bemrah, Z. Zendong, M.L. Morvan, P. Marchand, G. Dervilly-Pinel, J.P. Antignac, J.C. Leblanc, B. Le Bizec, Development and validation of a specific and sensitive gas chromatography tandem mass spectrometry method for the determination of bisphenol A residues in a large set of food items, J. Chromatogr. A 1362 (2014) 241–249.
[12] A. ter Halle, C. Claparols, J.C. Garrigues, S. Franceschi-Messant, E. Perez, Development of an extraction method based on new porous organogel materials coupled with liquid chromatography–mass spectrometry for the rapid quantification of bisphenol A in urine, J. Chromatogr. A 1414 (2015) 1–9.
[13] S.-H. Zhang, Y.-X. Zhang, G.-X. Ji, H.-Z. Xu, J.-N. Liu, L.-L. Shi, Determination of bisphenol A, tetrabromobisphenol A and 4-tert-octylphenol in children and adults

urine using high performance liquid chromatography-tandem mass spectrometry, Chin. J. Anal. Chem. 44 (1) (2016) 19–24.
[14] R. Kuruto-Niwa, Y. Tateoka, Y. Usuki, R. Nozawa, Measurement of bisphenol A concentrations in human colostrums, Chemosphere 66 (6) (2007) 1160–1164.
[15] H. Yin, Y. Zhou, S. Ai, R. Han, T. Tang, L. Zhu, Electrochemical behavior of bisphenol A at glassy carbon electrode modified with gold nanoparticles, silk fibroin, and PAMAM dendrimers, Microchim. Acta 170 (1-2) (2010) 99–105.
[16] Y. Zhang, T. Cao, X. Huang, M. Liu, H. Shi, G. Zhao, A visible-light driven photoelectrochemical aptasensor for endocrine disrupting chemicals bisphenol A with high sensitivity and specificity, Electroanalysis 25 (7) (2013) 1787–1795.
[17] X. Xu, D. Liu, L. Luo, L. Li, K. Wang, T. You, Photoelectrochemical aptasensor based on CdTe quantum dots-single walled carbon nanohorns for the sensitive detection of streptomycin, Sensors Actuat. B Chem. 251 (2017) 564–571.
[18] J. Li, Z. Dai, H. Li, Controllable Mn-doped ZnO nanorods for direct assembly of a photoelectrochemical aptasensor, Analyst 142 (12) (2017) 2177–2184.
[19] G. Wen, H. Ju, Enhanced photoelectrochemical proximity assay for highly selective protein detection in biological matrixes, Anal. Chem. 88 (16) (2016) 8339–8345.
[20] H. Li, J. Li, Y. Qiao, H. Fang, D. Fan, W. Wang, Nano-gold plasmon coupled with dual-function quercetin for enhanced photoelectrochemical aptasensor of tetracycline, Sensors Actuat. B Chem. 243 (2017) 1027–1033.
[21] X. Liu, P. Liu, Y. Tang, L. Yang, L. Li, Z. Qi, D. Li, D.K.Y. Wong, A photoelectrochemical aptasensor based on a 3D flower-like TiO_2-MoS_2-gold nanoparticle heterostructure for detection of kanamycin, Biosens. Bioelectron. 112 (2018) 193–201.
[22] J. Lv, Q. Lei, Q. Xiao, X. Li, Y. Huang, H. Li, Facile fabrication of “off-on” photoelectrochemical aptasensor for kanamycin detection based on polypyrrole/CeO_2, Anal. Methods 9 (2017) 4754–4759.
[23] Y. Yan, H. Li, Q. Liu, N. Hao, H. Mao, K. Wang, A facile strategy to construct pure thiophene-sulfur-dopedgraphene/ZnO nanoplates sensitized structure for fabricating a novel “on-off-on” switch photoelectrochemical aptasensor, Sensors Actuat. B Chem. 251 (2017) 99–107.
[24] Y. Liu, H. Ma, Y. Zhang, X. Pang, D. Fan, D. Wu, Q. Wei, Visible light photoelectrochemical aptasensor for denosine detection based on CdS/PPy/g-C_3N_4 nanocomposites, Biosens. Bioelectron. 86 (2016) 439–445.
[25] Y. Li, J. Tian, T. Yuan, P.o. Wang, J. Lu, A sensitive photoelectrochemical aptasensor for oxytetracycline based on a signal “switch off-on” strategy, Sensors Actuat. B Chem. 240 (2017) 785–792.
[26] Z. Dai, J. Guo, J. Xu, C. Liu, Z. Gao, Y.-Y. Song, Target-driven nanozyme growth in TiO_2 nanochannels for improving selectivity in electrochemical biosensing, Anal. Chem. 92 (14) (2020) 10033–10041.
[27] X. Jian, J. Xu, L. Yang, C. Zhao, J. Xu, Z. Gao, Y.Y. Song, Intracellular metal–organic frameworks: integrating an all-in-one semiconductor electrode chip for therapy, capture, and quantification of circulating tumor cells, Anal. Chem. 92 (2020) 13319–13326.
[28] M. Amouzadeh Tabrizi, M. Shamsipur, R. Saber, S. Sarkar, V. Ebrahimi, A high sensitive visible light-driven photoelectrochemical aptasensor for shrimp allergen tropomyosin detection using graphitic carbon nitride-TiO_2 nanocomposite, Biosens. Bioelectron. 98 (2017) 113–118.
[29] M. Zhu, C. Zhai, M. Sun, Y. Hu, B. Yan, Y. Du, Ultrathin graphitic C_3N_4 nanosheet as a promising visible-light-activated support for boosting photoelectrocatalytic methanol oxidation, Appl. Catal. B: Environ. 203 (2017) 108–115.
[30] J. Hu, C. Yu, C. Zhai, S. Hu, Y. Wang, N. Fu, L. Zeng, M. Zhu, 2D/1D heterostructure of g-C_3N_4 nanosheets/CdS nanowires as effective photo-activated support for photoelectrocatalytic oxidation of methanol, Catal. Today 315 (2018) 36–45.
[31] X. Jian, Y. Li, C. Zhao, Y. Chang, Z. Gao, Y.-Y. Song, Introducing graphitic carbon nitride nanosheets as supersandwich-type assembly on porous electrode for ultrasensitive electrochemiluminescence immunosensing, Anal. Chim. Acta 1097 (2020) 62–70.
[32] Y. Tang, Y. Chai, X. Liu, L. Li, L. Yang, P. Liu, Y. Zhou, H. Ju, Y. Cheng, A photoelectrochemical aptasensor constructed with core-shell CuS-TiO_2 heterostructure for detection of microcystin-LR, Biosens. Bioelectron. 117 (2018) 224–231.
[33] S.u. Liu, X. Xing, J. Yu, W. Lian, J. Li, M. Cui, J. Huang, A novel label-free electrochemical aptasensor based on graphene–polyaniline composite film for dopamine determination, Biosens. Bioelectron. 36 (1) (2012) 186–191.
[34] L. Huang, X. Yang, C. Qi, X. Niu, C. Zhao, X. Zhao, D. Shangguan, Y. Yang, A label-free electrochemical biosensor based on a DNA aptamer against codeine, Anal. Chim. Acta 787 (2013) 203–210.
[35] B. Deng, Y. Lin, C. Wang, F. Li, Z. Wang, H. Zhang, X.-F. Li, X.C. Le, Aptamer binding assays for proteins: the thrombin example—a review, Anal. Chim. Acta 837 (2014) 1–15.
[36] Z.R. Marand, N. Shahtahmassebi, M.R. Housaindokht, G.H. Rounaghi, I. Razavipanah, Construction of an amperometric glucose biosensor by immobilization of glucose oxidase on nanocomposite at the surface of FTO electrode, Electroanalysis 26 (4) (2014) 840–848.
[37] R.C. Dante, P. Martín-Ramos, A. Correa-Guimaraes, J. Martín-Gil, Synthesis of graphitic carbon nitride by reaction of melamine and uric acid, Mater. Chem. Phys. 130 (3) (2011) 1094–1102.
[38] J. Xu, Y. Wang, Y. Zhu, Nanoporous graphitic carbon nitride with enhanced photocatalytic performance, Langmuir 29 (33) (2013) 10566–10572.
[39] M. Karimi-Nazarabad, E.K. Goharshadi, Highly efficient photocatalytic and photoelectroncatalytic activity of solar light driven WO_3/g-C_3N_4 nanocomposite, Sol. Energy Mater. Sol. Cells 160 (2017) 484–493.
[40] A. Thomas, A. Fischer, F. Goettmann, M. Antonietti, J.-O. Muller, R. Schlogl, J.M. Carlsson, Graphitic carbon nitride materials: variation of structure and morphology and their use as metal-free catalysts, J. Mater. Chem. 18 (2008) 4893–4908.
[41] X. Bai, L.i. Wang, R. Zong, Y. Zhu, Photocatalytic activity enhanced via g-C_3N_4 nanoplates to nanorods, J. Phys. Chem. C 117 (19) (2013) 9952–9961.
[42] A. Thamri, H. Baccar, C. Struzzi, C. Bittencourt, A. Abdelghani, E. Llobet, MHDA-functionalized multiwall carbon nanotubes for detecting non-aromatic VOCs, Sci. Rep. 6 (2016) 1–12.
[43] W. Hou, S.B. Cronin, A review of surface plasmon resonance-enhanced photocatalysis, Adv. Funct. Mater. 23 (2013) 1612–1619.
[44] Z. Zhang, L. Zhang, M.N. Hedhili, H. Zhang, P. Wang, Plasmonic gold nanocrystals coupled with photonic crystal seamlessly on TiO2 nanotube photoelectrodes for efficient visible light photoelectrochemical water splitting, Nano Lett. 13 (1) (2013) 14–20.
[45] L. Fan, G. Zhao, H. Shi, M. Liu, Z. Li, A highly selective electrochemical impedance spectroscopy-based aptasensor for sensitive detection of acetamiprid, Biosens. Bioelectron. 43 (2013) 12–18.
[46] R. Shi, J. Liang, Z. Zhao, A. Liu, Y. Tian, An electrochemical bisphenol A sensor based on one step electrochemical reduction of cuprous oxide wrapped graphene oxide nanoparticles modified electrode, Talanta 169 (2017) 37–43.
[47] N. Ben Messaoud, M.E. Ghica, C. Dridi, M. Ben Ali, C.M.A. Brett, Electrochemical sensor based on multiwalled carbon nanotube andgold nanoparticle modified electrode for the sensitive detection of bisphenol A, Sensors Actuat. B Chem. 253 (2017) 513–522.
[48] H. Fan, Y. Li, D. Wu, H. Ma, K. Mao, D. Fan, B. Du, H.e. Li, Q. Wei, Electrochemical bisphenol A sensor based on N-doped graphene sheets, Anal. Chim. Acta 711 (2012) 24–28.
[49] B. Su, H. Shao, N.a. Li, X. Chen, Z. Cai, X.i. Chen, A sensitive bisphenol A voltammetric sensor relying on AuPd nanoparticles/graphene composites modified glassy carbon electrode, Talanta 166 (2017) 126–132.
[50] T. Zhan, Y. Song, Z. Tan, W. Hou, Electrochemical bisphenol A sensor based on exfoliated Ni2Al-layereddouble hydroxide nanosheets modified electrode, Sensors Actuat. B Chem. 238 (2017) 962–971.